Astrometric deflections from gravitational wave memory accumulation over cosmological scales

Töre Boybeyi,[1,*] Vuk Mandic,[1,†] and Alexandros Papageorgiou[2,3,‡]

[1]*School of Physics and Astronomy, University of Minnesota, Minneapolis, Minnesota 55455, USA*
[2]*Particle Theory and Cosmology Group, Center for Theoretical Physics of the Universe, Institute for Basic Science (IBS), 34126 Daejeon, Republic of Korea*
[3]*Instituto de Física Téorica, UAM-CSIC, 28049, Madrid, Spain*

(Received 6 May 2024; accepted 29 July 2024; published 30 August 2024)

We study the impact of gravitational wave memory on the distribution of far away light sources in the sky. For the first time, we compute the buildup of small, but permanent tensor distortions of the metric over cosmological timescales using realistic models of compact binary coalescences whose rate of occurrence is extrapolated at $z \sim \mathcal{O}(1)$. This allows for a consistent computation of the random-walk-like evolution of gravitational wave memory which, in turn, is used to estimate the overall shape and magnitude of astrometric deflections of far away sources of light. We find that, for pulsar or quasar proper motions, the near-Earth contribution to the astrometric deflections dominates the result and the deflection is analogous to a stochastic gravitational wave memory background that is generally subdominant to the primary stochastic gravitational wave background. We find that this contribution can be within the reach of future surveys such as Theia. Finally, we also study the deviation of the presently observed angular distribution of quasars from perfect isotropy, which arises from the slow buildup of gravitational wave memory over the entire history of the Universe. In this case, we find that astrometric deflections depend on the entire light trajectory from the source to Earth, yielding a quadrupole pattern whose magnitude is unlikely to be within reach of the next generation of astrometric surveys due to shot noise and cosmic variance limitations.

DOI: 10.1103/PhysRevD.110.043047

I. INTRODUCTION

In the past few years, we have witnessed a flurry of exciting discoveries in gravitational wave (GW) astrophysics. Advanced LIGO (aLIGO) [1] and Advanced Virgo (aVirgo) [2] observations of mergers of binary black holes (BBHs) [3], binary neutron stars (BNSs) [4], and black hole–neutron star systems [5], as well as pulsar timing array (PTA) measurements of the stochastic gravitational wave background [6–9] have established GW astrophysics on firm ground. They have also paved the way for a host of new tests of fundamental physics, such as tests of general relativity [10,11], constraints on the nuclear matter equation of state in neutron stars [4], new measurements of the Hubble constant H_0 [12,13], estimates of the stochastic gravitational wave background (SGWB) from BBH [14,15] and BNS [16] systems, constraints on dark matter from primordial BBHs (PBBHs) [17], early Universe scenarios [18], and more.

Despite achieving nearly 100 detections of GWs from BBH systems to date [19], at least one well-established prediction of general relativity remains elusive: gravitational wave memory (GWM). At its core, GWM is a phenomenon that entails a permanent change in the displacements of freely falling masses due to the passage of a GW. Observing GWM with terrestrial GW detectors such as aLIGO and aVirgo is challenging due to the relatively low-frequency nature of GWM, below the sensitive band of current terrestrial detectors while LIGO A# might detect GWM and the next generation terrestrial detectors like Einstein Telescope and Cosmic Explorer will certainly be able to do so [20,21]. On the other hand, it is possible that GWM could be detected using an ensemble of (∼2000) BBH mergers with current terrestrial detectors [22,23]. Space-based detectors such as LISA have a higher potential for detecting GWM [24–26], Also, PTA experiments have already placed strong upper limits on the GWM strain [27]. The linear form of GWM has been known since the 1970s [28–30] with the nonlinear form discovered in the 1990s [31,32]. Since then, our understanding and modeling of GWM has improved further [33–41] (see also [24] for a review) and deeper relationships between GWM, soft theorems, and Bondi-Metzner-Sachs transformations (infrared triangle) have been unveiled [42].

Most of the literature on GWM has focused on investigating the properties of GWM arising from individual

*Contact author: boybe001@umn.edu
†Contact author: vuk@umn.edu
‡Contact author: papageorgiou.hep@gmail.com

events such as from BBH mergers [43] or cosmic strings [44], and these studies roughly suggest that the GWM amplitude is expected to be an order of magnitude lower than the magnitude of the parent GW signal. Only relatively recently (beginning with [45]) several authors have begun investigating the phenomenology of stacking multiple GWM signals [45–48]. Unlike the previous studies, the purpose of the present work is to investigate the properties of the accumulated GWM in a patch of space arising from all possible sources over cosmological timescales and their impact on astrometric deflections. The basis of our work is the fact that a single GW burst with memory will cause a transient (primary GW) and permanent (GWM) change in the metric within a patch of space under consideration. Both effects consist of "stretching" one direction while "shrinking" another. However, the transient, although a stronger effect, will eventually decay away, while the weaker contribution will leave a permanent metric distortion in the patch of space under consideration. One can then consider the buildup of GWM over cosmological timescales by adding the GWM contributions from all GW sources in the history of the Universe, modeling each contribution as a steplike, permanent, quadrupolar distortion of spacetime. The effect described above can be conceptualized as a Brownian motion of stretching and shrinking of spacetime, with the mean metric distortion averaging to zero, but with a standard deviation that scales as the square root of the number of GW sources/events. The sheer number of events over the entire cosmological history of the Universe make it so this GWM accumulation could lead to deviations from isotropic expansion [48], cause redshift and deflections of light from distant sources such as quasars [49], and even cause distortions of the cosmic microwave background (CMB) [50]. Our work aims to establish the foundations for a more systematic understanding of the phenomenology of cumulative GWM and, to that end, we specifically focus on astrometric deflections as a first step.

When embarking on the calculation of accumulated GWM, one should, in principle, sum over all possible GW sources throughout the history of the Universe. This would include contributions of SGWB from inflation [51–57], early Universe phase transitions [58–66], additional "stiff" phases of cosmological evolution [67], cosmic strings [68–78], and GWs produced by recent astrophysical processes [14,16,79–102]. Performing a complete calculation that will include all possible sources is a daunting task, as it would involve modeling sources of GWs with very large uncertainties such as the cosmological SGWB (from inflation, cosmic strings, and phase transitions). We limit the scope of our analysis to contributions arising from mergers of compact objects such as BBHs, supermassive BBHs (SBBHs), and PBBHs, as the modeling of GWM strain for such sources in terms of the parameters of the primary GWs is well understood. In the case of BBHs of stellar origin, the local merger rate is well measured by aLIGO and aVirgo observations, and the redshift evolution of the BBH population can be modeled well using star formation rate [103,104]. In the case of SBBHs and PBBHs, both the local merger rate and its extrapolation to high redshifts are highly uncertain but constrained within certain limits [105,106]. Keeping all this in mind, our calculation of accumulated GWM should be understood as a lower limit since we are neglecting a plethora of other GW sources that would increase the overall GWM.

Given a model for the rate of accumulation of memory in the patch of space of interest, perhaps the most immediate and compelling phenomenological application is its potential impact on astrometric surveys of far away sources such as those performed already by Gaia [107–111] or the planned Telescope for Habitable Exoplanets and Interstellar/Intergalactic Astronomy (Theia) [112–114]. As is well established [49], a single gravitational wave burst with memory causes a deflection in the angular distribution of light sources in the sky. This deflection consists of two terms, coined the "Earth" and "star" terms. For the primary GW, the Earth term dominates, while the star term is strongly suppressed. On the other hand, for GWM the Earth and star terms can be comparable and the permanent deflections induced by GWM may depend on the entire history of the Universe. Our primary aim is to provide a realistic calculation for the memory buildup over cosmological scales and hence for the total astrometric deflection buildup which, in principle, could be imprinted in the statistics of the distant light sources proper motions or angular distributions. The physics of GWM in the context of astrometric deflections is complementary to the astrometric deflections by primary SGWB that have been studied extensively in the literature [115–119].

This work is organized as follows: In Sec. II, we outline the formalism that allows us to compute the accumulation of GWM over cosmological scales for different types of black hole binaries. In Sec. III, we provide the details needed for accurately modeling the binary merger rates and mass distributions for the BBH, SBBH, and PBBH populations. In Sec. IV, we show the results of our numerical analysis, computing the GWM for different populations of binaries. In Sec. V, we discuss detection prospects for cumulative GWM focusing on astrometric deflections, and we conclude in Sec. VI. We will set $c = 1$.

II. GWM ACCUMULATION

As outlined above, one key difference between the primary GW and GWM is that the former is transient, while the latter is permanent. As a result, we expect the latter to accumulate over time. We focus our attention to a small patch of space whose memory accumulation, over cosmological timescales, we want to compute. The patch of space is sufficiently small compared to the distance to the sources of GWs, so that we can assume the GWM to be

homogeneous within it and the wavefronts to be planar. In this context, every GW signal arriving from a random direction and with random polarization will induce a small, but permanent, change in the metric in the chosen patch. Of course, such changes can have differing amplitudes and signs, implying that cumulative GWM evolves in a random walk fashion with zero mean and a standard deviation that scales as the square root of the number of GW sources. This cumulative random walk process results in small permanent metric fluctuations (anisotropy) from patch to patch [48], which may impact trajectories of light from distant sources [49,50] and cause apparent deflections of these sources on the sky.

The basic ingredient necessary for our calculation is the local merger rate per comoving volume in the source frame, which we denote as $R_X(z)$ where $X = \mathrm{BBH/SBBH/PBBH}$ is an index that specifies the source of GWs. The explicit form of $R_X(z)$ depends on the type of BBH population we consider, and we will specify it below for the three cases we consider. We then convert the merger rate to the observer frame by dividing by redshift and we further multiply by the differential comoving volume dV/dz to obtain the observer merger rate

$$R_{X,z}(z) = \frac{R_X(z)}{(1+z)}\frac{dV}{dz} = \frac{R_X(z)}{(1+z)}\frac{4\pi D^2(z)}{H_0 E(z)}, \tag{1}$$

where $D(z)$ is the comoving distance to the source and $E(z) = \sqrt{\Omega_m(1+z)^3 + \Omega_\Lambda}$ accounts for the expansion of the Universe with the standard energy densities of matter, $\Omega_m = 0.3$, and dark energy, $\Omega_\Lambda = 0.7$. Alternatively, $H(z) = H_0 E(z)$ is the Hubble constant as a function of time/redshift. We then generalize this rate into the merger rate as observed at a redshift z_o,

$$\tilde{R}_{X,z}(z_o, z_{so}) = \frac{R_X(z_s)}{(1+z_{so})}\frac{4\pi D^2(z_o, z_s)}{H_0 E(z_{so})}, \tag{2}$$

where we have defined z_{so} as the redshift of the source at z_s relative to the observing redshift z_o,

$$1 + z_{so} = \frac{1+z_s}{1+z_o}. \tag{3}$$

In order to compute the total GWM in the given patch accumulated over the entire history, one needs to integrate the GWM contributions generated by GWs arriving at each observer redshift z_o, which in turn depend on all GW sources at redshifts $z_s > z_o$. The integration region is depicted in Fig. 1.

In addition to the merger rate, one also needs the GWM strain for each individual event. We will employ the so-called "step model," $h(t) = \Theta(t - t_m)h_{+,\mathrm{mem}}(z_{so}, M, \theta)$, where $\Theta(t)$ denotes the Heaviside step function, t_m is the time of the merger, and $h_{+,\mathrm{mem}}$ denotes the amplitude of the memory signal. This approximation is generally appropriate for timescales much larger than the merger timescale that we will be interested in for compact binaries. For compact binary mergers in circular orbits, the plus polarization of the amplitude of GWM is typically dominant and is well approximated by [41]

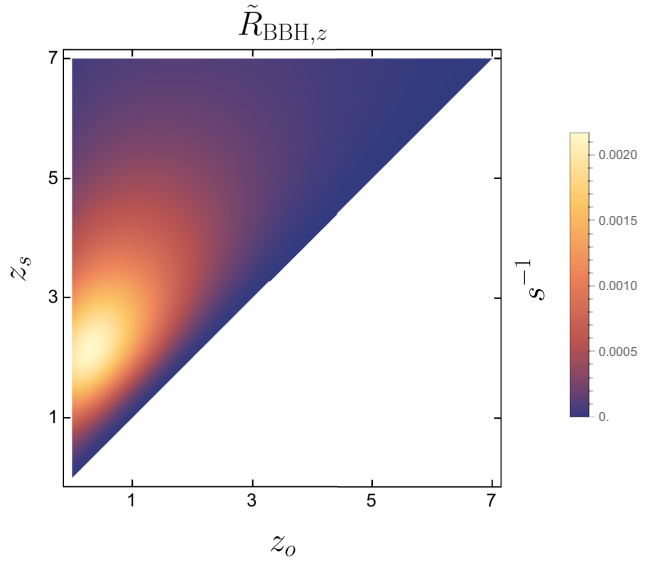

FIG. 1. Cumulative GWM calculation integrates all GWM contributions from all sources over the entire history of the Universe, as depicted by the shaded triangular region. Here we display the merger rate for stellar BBH population defined in Eq. (2).

$$h_{+,\mathrm{mem}}(z_{so}, M, \theta) = \frac{GM}{144 D(z_o, z_s)}\zeta(\theta), \tag{4}$$

where $D(z_o, z_s)$ is the comoving distance to the GW source to an observer at $z = z_o$, θ is the angle between the binary's orbital plane and the binary's location in the sky, and M is the mass of a component black hole of the binary system, assuming the two component black holes have the same mass. The angular factor is given in [41] as $\zeta(\theta) = \sqrt{2}(17 + \cos^2\theta)\sin^2\theta$.

Note that, for simplicity, we multiplied the result due to the inspiraling phase by a factor of 2 to model the contribution of the ringdown phase. This is a rough approximation that is sufficient to get the correct order of magnitude and it significantly simplifies the expressions we use below. Note also that we assumed the masses of the two compact objects to be the same for simplicity.

Finally, in addition to the above, we need a mass distribution from which we draw a random value for the mass of the black holes for each event. We denote the probability distribution as $g_X(M)$ and assume it to be independent of the redshift for simplicity.

The elements outlined above can be used to sum the total GWM over cosmological scales. Specifically, we assume

that strain h_+ occurs at a rate $\tilde{R}_{X,z}(z_o, z_{so})$, with a uniformly distributed inclination angle θ and direction in the sky and with a mass drawn from distribution $g_X(M)$.

We use the formalism in [120] to express the SGWB in terms of merger rate as observed at a redshift z_o,

$$\Omega_{\rm mem}(f, z_o) = \frac{f}{\rho_c H_0}\int_0^\infty dz_{so}\frac{R_X(z_s)\langle\frac{dE_{\rm mem}}{df}(f_s, z_{so})\rangle}{(1+z_{so})\sqrt{\Omega_\Lambda+\Omega_{\rm M}(1+z_{so})^3}}, \quad (5)$$

where $\rho_c = 3H_0^2/8\pi G$ and $f_s = f(1+z_s)$ is frequency of the GW evaluated at the source. The ensemble average denoted by brackets means averaging over the mass and angular distributions given by $\langle\ldots\rangle = \int d\phi d\theta \sin(\theta)\int dM g_X(M)$. In the step model and using Eq. (4), we have

$$h(f) = \frac{1}{2\pi i f}\frac{GM}{144 D(z_o, z_s)}\zeta(\theta) \quad (6)$$

up to a Dirac-δ function at $f = 0$, which is not relevant for the following derivations, and [121]

$$\frac{dE_{\rm mem}}{df}(f_s, z_{so}) = \frac{\pi^2}{G}D^2(z_o, z_s)(1+z_s)^2 f^2 |h(f(1+z_s))|^2. \quad (7)$$

Combining these,

$$\Omega_{\rm mem}(f, z_o) = f\frac{2\pi G^2}{3H_0^3}\frac{\sigma_\theta^2}{(144^2)}\int dM\, M^2 g_X(M) \times\int_0^\infty dz_{so}\frac{R_X(z_s)}{(1+z_{so})\sqrt{\Omega_\Lambda+\Omega_{\rm M}(1+z_{so})^3}}, \quad (8)$$

where

$$\sigma_\theta^2 = \int_0^\pi d\theta\, \sin(\theta)\zeta(\theta)^2 \simeq 627, \quad (9)$$

denoting the angular contribution. The lower limit of the dz_{so} integral is chosen to be zero, which implies that the patch under consideration, whose memory can be understood as homogeneous, is infinitesimal in size. If one wants to consider finite size patches, the lower limit should be adjusted to ensure that the sources of gravitational waves are much farther away than the characteristic patch size.

In the next section, we compute the $\Omega_{\rm mem}(f, z_o)$ for different populations of binaries and then use it to numerically compute the total memory accumulation over cosmological scales.

III. SOURCES OF GWM AND MERGER RATES

We dedicate this section to computing the merge rates and mass distribution for three types of binary black holes: BBHs, PBBHs, and SBBHs. In particular, for each of the three populations we specify the model and parameters for the merger rate $R_X(z)$ and the mass distribution $g_X(M)$, enabling the computation of Eq. (8). Table I lists the ranges of relevant parameters used in the three population models.

A. Binary black hole mergers

Binary black hole systems of stellar origin are well constrained by ground-based GW detectors and their properties are relatively well understood. We assume that the BBH merger rate follows the star formation rate (SFR) [122],

$$R_{\rm BBH}(z) = \nu\frac{p e^{q(z-z_m)}}{(p-q)+q e^{p(z-z_m)}}, \quad (10)$$

with the parameter ν normalizing the merger rate to the observed merger rate at $z = 0.2$. The peak of the SFR is defined by z_m, while $p-q$ and q define slopes of SFR at high and low redshifts. We have chosen the range of these parameters (see Table I) so that they are consistent with the LIGO third observing run (O3) results [123]. We draw free

TABLE I. Population model parameters. Here $\mathcal{N}(\mu, \sigma)$ denotes normal distribution, whereas $U_{[a,b]}$ denotes the uniform distribution.

Parameters	Range/value
BBH parameters	
$\nu(\mathrm{Gpc^{-3}\,yr^{-1}})$	$\mathcal{N}(150, 10^2)$
p	$\mathcal{N}(2.37, 0.1^2)$
z_m	$\mathcal{U}_{[2.0,2.4]}$
q	$\mathcal{N}(1.8, 0.1^2)$
m	$\mathcal{U}_{[2.0,2.4]}$
$\bar{M}$	$30M_\odot$
σ_m	$5M_\odot$
M_l	$5M_\odot$
M_h	$\mathcal{U}_{[80,100]M_\odot}$
PBBH parameters	
M_c	$\mathcal{U}_{[25,30]M_\odot}$
σ_M	$\mathcal{U}_{[0.1,0.3]M_\odot}$
$f_{\rm sup}$	10^{-3}
α	$\mathcal{U}_{[1.0,1.6]}$
$f_{\rm PBH}$	$\mathcal{U}_{[0,1]}$
SBBH parameters	
$\log_{10}\frac{\dot{n}_0}{(\mathrm{Mpc^{-3}\,Gyr^{-1}})}$	$\mathcal{N}(-3, 1)$
α_M	$\mathcal{U}_{[-2,2]}$
$\log_{10}\frac{M_*}{M_\odot}$	$\mathcal{U}_{[6.5,8.5]}$
β_z	$\mathcal{U}_{[0,7]}$
z_c	$\mathcal{U}_{[0,5]}$

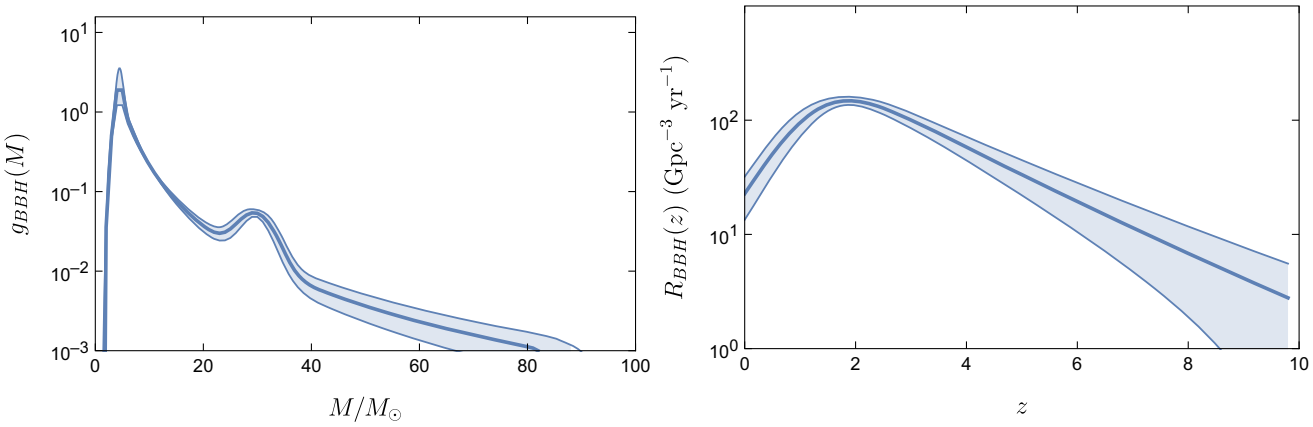

FIG. 2. Mass distribution (left) and merger rate (right) for BBHs using the models in Eqs. (11) and (10) with values in Table I. Bands denote the 1-σ (68%) confidence region, computed as described in the text.

parameters of the BBH merger rate model from their distributions given in Table I, calculate $R_{\rm BBH}(z)$ for each parameters choice, and plot the 68% confidence region of computed $R_{\rm BBH}(z)$ curves in Fig. 2 (right).

The BBH mass distribution is assumed to follow the power-law peak model with the lower cutoff at $5M_\odot$ and high cutoff around $[80, 100]M_\odot$,

$$g_{\rm BBH}(M) = \left((1-\lambda)\frac{M^{-m}}{\lambda_1} + \lambda\frac{e^{-(M-\bar{M})^2/(2\sigma_M^2)}}{\lambda_2}\right) \times \Theta(M_h - M)\Theta(M - M_l). \tag{11}$$

Here, λ_1, λ_2 are normalization constants of the two distribution components and $\lambda = 0.08$ is the mixing factor. We assume the mass distribution does not evolve with redshift. Typical ranges of these parameters are given in Table I. Again the ranges of parameters are chosen to be in agreement with the LIGO O3 results [123].

Similar to the merger rate, we draw free parameters of the BBH mass model from their distributions given in Table I and calculate $g_{\rm BBH}(M)$ for each parameter choice, then plot with the corresponding 68% confidence region on the left side of Fig. 2.

B. Primordial binary black hole mergers

The primordial black hole mass distribution is highly uncertain. The lower limit on the primordial black holes masses today is the so-called Hawking evaporation limit ($10^{-18}M_\odot$), while binaries larger than $10^2M_\odot$ are highly constrained by CMB and other indirect observations (cf. Fig. 1 of [124]). Here, we will take the best case scenario and assume that the PBBH merger mass distribution is between $10^0M_\odot$ and $10^2M_\odot$, as these are the most massive primordial black holes that may enjoy large abundances in the present and recent past (and hence greater merger rates as we will show below). We assume their distribution to be log-normal as commonly done [125,126],

$$g_{\rm PBBH}(M) = \frac{1}{\sqrt{2\pi}\sigma_M M}\exp\left(-\frac{\log^2(M/M_c)}{2\sigma_M^2}\right) \tag{12}$$

where M_c is the peak mass of $Mg(M)$ and σ_M characterizes the width of the mass function. Log-normal distribution is usually motivated by baryonic dark matter models as proposed in [127].

While the mass distribution is different from the stellar BBH case, the more important difference is in the binary merger rate as a function of redshift. The PBBH systems do not follow the evolution of stellar material and are instead related to the evolution of dark matter halos. The PBBH merger rate has been studied in several works [125,128–132]. As an example, the formalism of [131] assumes a simple power-law dependence of the merger rate with redshift,

$$R_{\rm PBBH}(z) = R_{\rm PBBH}(0)(1+z)^\alpha, \tag{13}$$

with $\alpha \sim 1.3$ for a Poisson spatial distribution of the PBBH systems [106]. In this scenario, the local merger rate for equal mass black holes is given by [125,133]

$$\frac{R_{\rm PBBH}(z=0)}{\rm Gpc^{-3}\ yr^{-1}} = 4\times10^5 f_{\rm sup} f_{\rm PBH}^{53/37}\left(\frac{M}{M_\odot}\right)^{-32/37}, \tag{14}$$

where $f_{\rm PBH}$ is the fraction of dark matter in the form of primordial black holes ($\leq$1 by definition) and $f_{\rm sup}$ is a suppression factor that depends on the effects from other PBBHs and the matter distribution surrounding it. In [133], the value of $f_{\rm sup} \sim 10^{-3}$ (chosen to be a benchmark number) was argued to be consistent with current LIGO observations giving consistent merger rates and also motivated by N-body simulations.

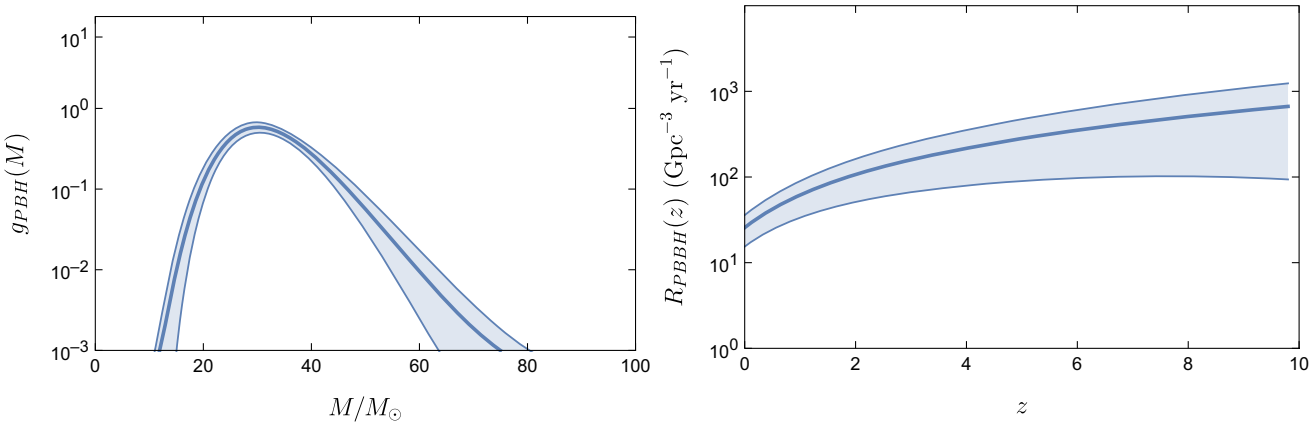

FIG. 3. Mass distribution (left) and merger rate [with $M = M_\odot$ in Eq. (14)] (right) for PBBHs using the models in Eqs. (12)–(14) with values in Table I. Bands denote the 1-σ (68%) confidence region, computed as described in the text.

Ranges for all of the free parameters of the PBBH model are chosen to be consistent with the SGWB estimates from LIGO in [131] and are given in Table I. The 68% confidence regions for the merger rate and mass models for PBBH are calculated in the same way as for the stellar BBH model and are plotted in Fig. 3. The resulting mass distribution in Fig. 3 is somewhat tight, likely due to the fact that LIGO sensitivity is optimal for binaries around the individual mass window of $(30, 60)M_\odot$ combined with the log-normal assumption that favors a narrow range of PBBHs. In fact, studies on individual loud events as in [134] also predict a similar distribution.

C. Supermassive binary black hole mergers

There are various models for SBBH mergers. The two most common models used in the literature are the so-called astrophysically informed [135] [$\dim(\theta_i) = 16$] and the agnostic/minimal [136] [$\dim(\theta_i) = 5$] models. Parameters of these models are constrained by PTA experiments, for example, in [137].

We will use the agnostic model outlined in [136–138] as it captures the essential properties of SBBH population while retaining simplicity. In this model, merger rate is given by a Schechter function,

$$R_{\mathrm{SBBH}}(z) = \dot{n}_0(1+z)^{\beta_z} e^{-z/z_c} \tag{15}$$

with mass probability density

$$g_{\mathrm{SBBH}}(M) = \frac{1}{M}\left(\frac{M}{10^7 M_\odot}\right)^{-\alpha_M} e^{-M/M_\star}. \tag{16}$$

The agnostic model is based on the assumption that binary systems undergo mergers in circular orbits, influenced only by radiation reaction. The density of these mergers, denoted by $\dot{n}_0$, is measured per unit of rest-frame time and comoving volume. For the distribution's characteristics in terms of M, the parameters α_M and $M_\star$ specify the slope and the cutoff point, respectively. Meanwhile, the distribution in z is similarly defined by the parameters

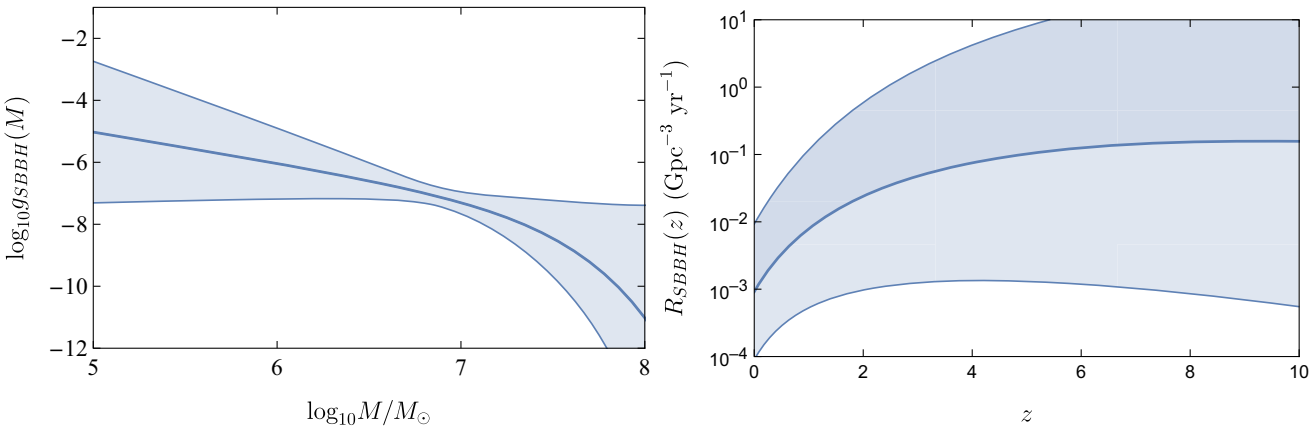

FIG. 4. Mass distribution (left) and merger rate (right) for SBBHs using the models in Eqs. (15) and (16) with values in Table I. Bands denote the 1-σ (68%) confidence region, computed as described in the text.

β_z and z_c, which represent the same features for the merger rate.

The ranges of all free parameters of the SBBH model are chosen to obey the PTA constraints [136–138] and are given in Table I. The 68% confidence regions for the SBBH merger rate and mass models are calculated in the same way as in the previous cases and are plotted in Fig. 4.

IV. CUMULATIVE GWM ESTIMATES

Memory accumulation can be characterized by a 1D random walk. The step size at each time is a Gaussian random variable with zero mean and a time-dependent variance $\sigma(t)$. Probability of accumulating memory strain h after time t is given by

$$P(h) \propto \exp\left(-\frac{h^2}{2\sigma^2(t)}\right). \tag{17}$$

We define the so-called diffusion constant, which is an invariant characterization for random walks, by $D(t) = \dot{\sigma}\sigma$, where the dot represents the time derivative.

We note that the diffusion constant is itself a function of time in our case. The time evolution and the amplitude of the diffusion constant depend on the parameters of the population/merger rate model outlined in the previous section. Each realization of the population is a set of random parameters drawn from the distributions given in Table I. Therefore, each realization yields a different curve $D(z_o)$.

We relate the diffusion constant to the stochastic gravitational wave background due to memory. The power spectral density for a random walk is given by

$$S_{\rm mem}(f) = \frac{D}{\pi^2 f^2}, \tag{18}$$

valid for frequencies lower than the merger timescale of the binaries. Combining this with the standard relationship between the strain power spectrum and the energy density of the stochastic background,

$$\Omega_{\rm mem}(f) = \frac{4\pi^2 f^3 S_{\rm mem}(f)}{3H_0^2} \tag{19}$$

yields

$$\Omega_{\rm mem}(f) = \frac{4Df}{3H_0^2}. \tag{20}$$

This in our case generalizes to

$$\Omega_{\rm mem}(f, z_o) = \frac{4D(z_o)f}{3H_0^2}, \tag{21}$$

where $\Omega_{\rm mem}(f, z_o)$ is given by Eq. (8).

On the left side of Fig. 5, we show the evolution of the diffusion constant for the three GW source populations: BBHs, PBBHs, and SBBHs. The bands of each source correspond to 1-σ interval, i.e., the regions in which the central 68% of the $D(z_o)$ curves lie. The central solid curves are the mean of the realizations. The present time diffusion constant values $D(0)$ are comparable to previous results [47], which did not investigate the redshift dependence of the memory accumulation process. Our results, therefore, extrapolate $D(0)$ to high redshifts.

Having the full $D(z_o)$, one can make an estimate of the typical strain accumulation h_c, which is given by the symmetric Gaussian distribution defined in Eq. (17). More precisely, the typical magnitude of h_c is given by the diffusion length, defined as

$$h_c \approx 2\sqrt{\int_{z_o=10}^{z=0} D(t)dt}. \tag{22}$$

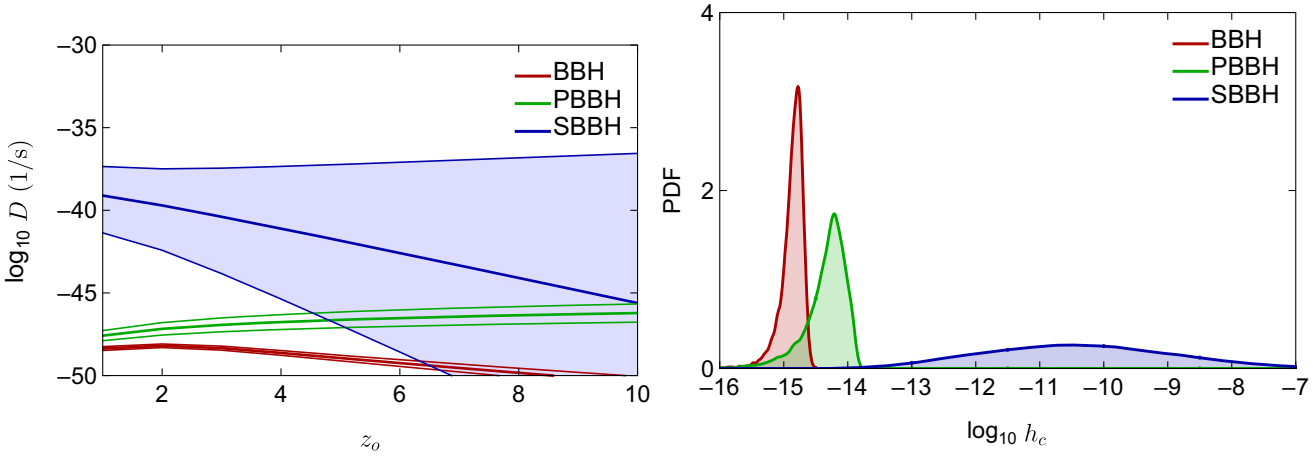

FIG. 5. Diffusion constant D as a function of redshift along with its 1-σ (68%) confidence region (left) and corresponding diffusion length probability distribution (right).

Figure 5 (right) shows the probability distribution of h_c for different sources. We note that SBBH sources would dominate the cumulative memory effects (reaching the effective strain 10^{-11}–10^{-9}) as compared to the BBH and PBBH models, with ∼4 orders of magnitude uncertainty in the diffusion length today due to the large uncertainty in the SBBH population model.

V. ASTROMETRIC DEFLECTIONS

One compelling application for the GWM accumulation derived in the preceding section is the contribution to astrometric deflections of far away objects such as pulsars or quasars. Our work is based on the treatment of astrometric deflections by GWs and GWM by Madison [49], which makes use of the formalism of Book and Flanagan [139]. The observed angular deflection of a distant light source located at n^i, due to a propagating tensor perturbation, can be expressed as Eq. (35) of [139],

$$\delta n^i = P^{ik} n^j \left(-\frac{h_{jk}(0)}{2} + \frac{p_k n_l}{2(1+\boldsymbol{p}\cdot\boldsymbol{n})} h_{jl}(0) + \frac{1}{\lambda_s}\int_0^{\lambda_s} d\lambda \left[h_{jk}(\lambda) - \frac{p_k n_l}{2(1+\boldsymbol{p}\cdot\boldsymbol{n})} h_{jl}(\lambda) \right] \right) \tag{23}$$

with $P^{ik} = \delta^{ik} - n^i n^k$ being the transverse-traceless projector and $h_{ij}(\lambda) = \epsilon^A_{ij}(\boldsymbol{p}) h(t - \lambda(1+\boldsymbol{p}\cdot\boldsymbol{n}))$ is the strain evaluated on the unperturbed path at an earlier time with p^i denoting the wave direction. Here, λ_s is the proper distance to the light source and the source of the tensor perturbation is assumed to be much further away than λ_s so that the plane wavefront approximation holds. The expression coincides with the one for an expanding Universe [139] up to an overall scale factor correction, which we take to be 1 since we will consider only gravitational wave sources with $\mathcal{O}(1)$ redshift. This can be simplified and subsequently split in terms of Earth and star contributions [Eq. (5) of [49]],

$$\delta n^i(t) = \mathcal{V}^{i,A}_{\oplus}(\boldsymbol{p}) h(t) + \mathcal{V}^{i,A}_{\star}(\boldsymbol{p}) \frac{H(t) - H(t - \lambda_s(1+\boldsymbol{p}\cdot\boldsymbol{n}))}{\lambda_s(1+\boldsymbol{p}\cdot\boldsymbol{n})} \tag{24}$$

with

$$\mathcal{V}^{i,A}_{\oplus}(\boldsymbol{p}) = -\frac{n^j \epsilon^{i,A}_j}{2} + n^l n^j \epsilon^A_{jl} \left[\frac{p^i + n^i}{2(1+\boldsymbol{p}\cdot\boldsymbol{n})} \right], \tag{25}$$

$$\mathcal{V}^{i,A}_{\star}(\boldsymbol{p}) = n^j \epsilon^{i,A}_j - \frac{n^i n^l n^j \epsilon^A_{jl}}{2} - n^l n^j \epsilon^A_{jl} \left[\frac{p^i + n^i}{2(1+\boldsymbol{p}\cdot\boldsymbol{n})} \right], \tag{26}$$

where $H = \int h(\lambda) d\lambda$ and $A = +, \times$ is the polarization index. The star term encapsulates propagation effects, while the Earth term captures the deflection due to the strain at the observer location. The deflection patterns of the Earth term $\mathcal{V}^{i,A}_{\oplus}$ for different polarizations are shown in Fig. 6.

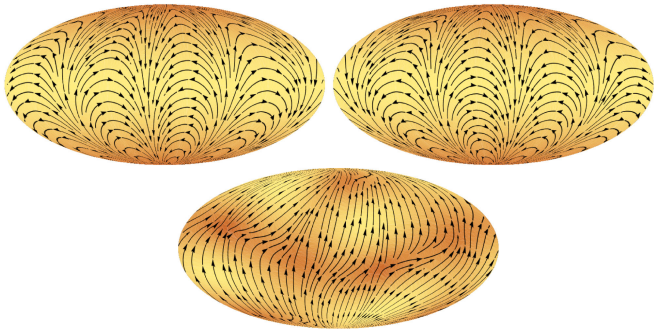

FIG. 6. Top two figures depict deflection patterns of + and × polarization of $\mathcal{V}^{+,\times}_{\oplus}$, respectively, for a GW propagating in the $\hat{z}$ direction. The bottom figure depicts a realization of deflection for many such GWs uniformly distributed in direction and polarization.

One interesting limit, which will be referred to as the "saturation limit," is defined as $\delta n^i_s \equiv \delta n^i(\infty)$ and corresponds to the final deflection configuration, long after the gravitational wave has passed over the local patch of space spanning the light source and observer. It is straightforward to calculate this limit from Eq. (24); letting $h(t) = A_0 \Theta(t)$, one obtains

$$\delta n^i_s(\infty) = A_0 (\mathcal{V}^{i,A}_{\oplus}(\boldsymbol{p}) + \mathcal{V}^{i,A}_{\star}(\boldsymbol{p})) = \frac{A_0}{2} P^{ij} \epsilon^A_{jk} n^k. \tag{27}$$

Paying particular attention to the memory part of the signal, it is important to note that its size is highly unsuppressed compared to the nonmemory part at late times. More specifically, From Eq. (24) one can see that unlike for regular GWs whose star term is suppressed by $\sim 1/\lambda_s$, the star term for GWM grows as $\sim t/\lambda_s$ and gradually becomes $\mathcal{O}(h)$. This in turn implies that, for GW signals that passed over Earth in recent years, one would expect the Earth term to yield the greatest contribution to the total astrometric deflection of a far away source. On the other hand, for GWs that passed over Earth long ago, the contribution of the star term is greater—i.e., in general, it can increase even after the primary wavefront has propagated beyond Earth. Eventually, if we consider GWs that passed over the patch of space defined by the light source and Earth even before the light was emitted (that we observe today), the overall effect of the astrometric deflection would be precisely the saturation limit we defined above. In that case, the light propagated through the already perturbed metric from the moment it was emitted until it finally arrived at Earth.

Because of the considerations outlined above, we separate our analysis into two distinct observational scenarios.

(i) Observations of the proper motion of far away sources through astrometric deflections during the observation time. In such a scenario, one would

compare how the location of sources of light, such as pulsars or quasars, changes over the timescale of the observations [e.g., $\mathcal{O}(10)$ yr]. The dominant contribution to this measurement will arise from the Earth term of GWs that propagate by Earth within the time of observation while the star term provides a small, low-frequency correction.

(ii) Observations of the angular distribution of far away sources, such as quasars, based on a single time snapshot. Deviation of this distribution from perfect isotropy could then be attributed to GWM, and we will analyze the statistics of such a deviation. In this scenario, the Earth and star terms contribute on the same order and GWs emitted throughout the history of the Universe are important.

For each of these scenarios, it is required to calculate the so-called geometric correlation function. We define it in the following way:

$$\Gamma^A_{ij,\oplus}(\boldsymbol{n},\boldsymbol{n}') = \int d^2\boldsymbol{p}\mathcal{V}^{i,A}_{\oplus}(\boldsymbol{n},\boldsymbol{p})(\mathcal{V}^{j,A}_{\oplus}(\boldsymbol{n}',\boldsymbol{p}))^* \quad (28)$$

for the Earth term and

$$\Gamma^A_{ij,\oplus+\star}(\boldsymbol{n},\boldsymbol{n}') = \int d^2\boldsymbol{p}(\mathcal{V}^{i,A}_{\oplus}(\boldsymbol{n},\boldsymbol{p}) + \mathcal{V}^{i,A}_{\star}(\boldsymbol{n},\boldsymbol{p})) \quad (29)$$

$$\times\ (\mathcal{V}^{j,A}_{\oplus}(\boldsymbol{n}',\boldsymbol{p}) + \mathcal{V}^{i,A}_{\star}(\boldsymbol{n},\boldsymbol{p}))^* \quad (30)$$

for the saturation limit. The above quantities are tensors, but for practical reasons it is more useful to expand them in a suitable basis with scalar coefficients. Let us define the following basis:

$$\boldsymbol{u}_y = \frac{(\boldsymbol{n}\times\boldsymbol{n}')}{\sqrt{1-(\boldsymbol{n}\cdot\boldsymbol{n}')^2}} \qquad \boldsymbol{u}_x = \boldsymbol{u}_y \times \boldsymbol{n}, \quad (31)$$

$$\boldsymbol{u}_\phi = \boldsymbol{u}_y \qquad \boldsymbol{u}_\theta = \boldsymbol{u}_\phi \times \boldsymbol{n}'. \quad (32)$$

There are four possible projections, for example, $\Gamma^A_{x\theta,\oplus} \equiv \Gamma^A_{ij}u^i_x u^j_\theta$, $\Gamma^A_{x\theta} \equiv \Gamma^A_{ij}u^i_y u^j_\phi$, etc. The nonzero projections of $\Gamma^A_{ij,\oplus}$ and $\Gamma^A_{ij,\oplus+\star}$ are shown in Fig. 7 with the definition $\cos(\Theta) = \boldsymbol{n}\cdot\boldsymbol{n}'$. Using these, one can reconstruct these tensor geometric two-point correlations as

$$\Gamma^A_{ij_\oplus}(\Theta) = \sum_{x_i=x,y.}\sum_{\theta_j=\theta,\phi.} \Gamma^A_{x_i\theta_{j\oplus}}(\Theta)u^i_{x_i}u^j_{\theta_j}, \quad (33)$$

$$\Gamma^A_{ij_{\oplus+\star}}(\Theta) = \sum_{x_i=x,y.}\sum_{\theta_j=\theta,\phi.} \Gamma^A_{x_i\theta_{i\oplus+\star}}(\Theta)u^i_{x_i}u^j_{\theta_j}. \quad (34)$$

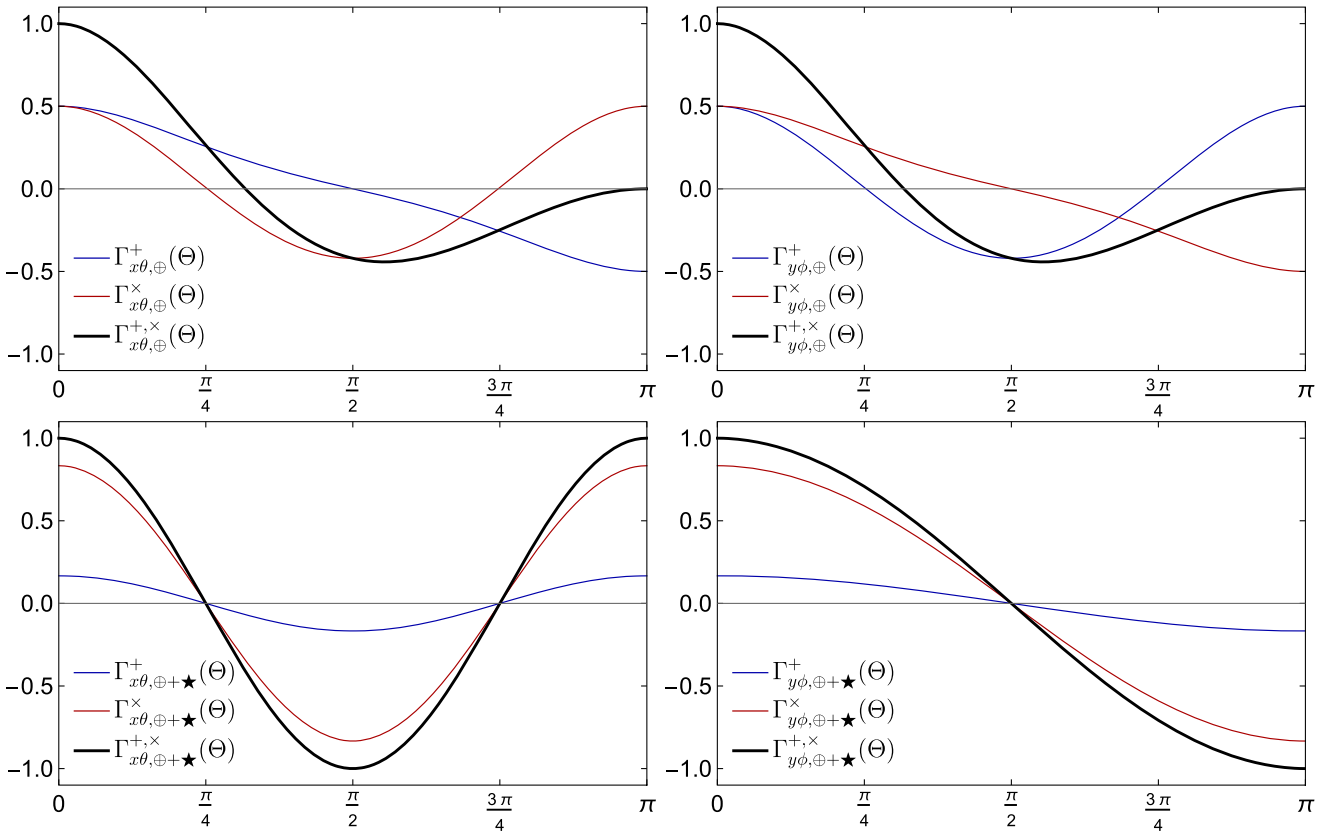

FIG. 7. Correlation function for the Earth term (top) given in Eq. (25) and the saturation limit (bottom) given in Eq. (27) are shown after expansion in orthogonal basis functions as defined in Eq. (31).

We observe that, in the case of the Earth term, the $\Gamma_{x\theta}$ and $\Gamma_{y\phi}$ correlation functions (with the polarizations exchanged) are identical. In the case of the star term, this degeneracy is broken and all contributions are distinct. As a final note, in this paper we are using conventions in [117] to set the basis vectors (see Refs. [117,139] for an analytical derivation of the Earth correlation function). The star term is usually neglected in the literature as it is multiplied by $H(t)$, which saturates to a finite value for oscillatory waves and as a result the star term is suppressed by $H(t)/\lambda_s$. In the case of the memory, however, the star term remains unsuppressed until it saturates to a final value comparable to the Earth term, as described by the saturation limit defined above.

A. Impact on the proper motions of far away objects

We dedicate this section to analyzing the first of the two scenarios to constrain GWM accumulation. We will focus on the dominant SBBH source. As mentioned above, the strategy is to compare the change of astrometric data of celestial objects in a certain data collection interval. An ideal source for such data is Gaia and Theia measurements with observation time $T \sim 10$ yr. In this scenario, the star term can be neglected. Starting from Eq. (23) and defining $\omega^i_{\rm gw} = \delta\dot{n}^i$, the equal-time two-point correlation of the proper motions due to a Gaussian isotropic stochastic background is given by [139]

$$\langle \omega^i_{\rm gw}(\boldsymbol{n}, t)\omega^j_{\rm gw}(\boldsymbol{n}', t)\rangle = \Gamma_{ij,\oplus}(\Theta)\omega^2_{\rm rms}, \tag{35}$$

where

$$\Gamma_{ij,\oplus}(\Theta) \equiv \sum_{A=+,\times} \Gamma^A_{ij,\oplus}(\Theta) \tag{36}$$

and

$$\omega^2_{\rm rms} \equiv H_0^2 \int_{f_{\rm low}}^{f_{\rm high}} d\ln f\, \Omega_{\rm mem}(f) \tag{37}$$

gives the rms of proper motions. Here, $\Omega_{\rm mem}(f) = \Omega_{\rm mem}(f, z_o = 0)$ is the energy density per unit logarithmic interval in gravitational wave background due to the memory as of now, related to the strain power spectrum via Eq. (19) [139]. Before going into further details of how this effect can be analyzed in a given dataset, it is beneficial to make a comparison between nonmemory and memory contributions to the SGWB, both of which contribute to the two-point correlation in the same way and with the same $\Gamma_{ij,\oplus}(\Theta)$. We note that, for a SGWB sourced by SBBH mergers,

$$\Omega_{\rm nonmem}(f) = A_0(f/{\rm yr}^{-1})^{2/3} \qquad f_{\rm low} \le f \le f_{\rm high},$$
$$\Omega_{\rm mem}(f) = \frac{4D(0)}{3H_0^2} f \qquad f_{\rm low} \le f \le f_{\rm high}, \tag{38}$$

where $A_0 \simeq 10^{-9}$ [140] and $D(0) = 10^{-38\pm2}$ s^{-1} as shown in the $z_0 \to 0$ limit for $D(z_0)$ for SBBH in Fig. 5 (left). We note that the model (38) for GWM is only an approximation that holds for frequencies smaller than inverse merger timescale.

The low-frequency cutoff is not relevant for this calculation since the integral of Eq. (37) is dominated by the high-frequency cutoff. For the high-frequency cutoff, we note that Gaia outputs data for a single proper motion over T. Therefore, motions above the frequency $2/T$ will be suppressed. Hence, we take $f_{\rm high} = 2/T \sim 10^{-8}$ Hz to be the same for nonmemory and memory as well. We also point out that inverse merger timescale for an equal mass $M = 10^{10}M_\odot$ binary is $\frac{c^3}{2GM} \sim 10^{-5}$ Hz, which is much larger than the cutoff we are using above; therefore, the step model should be a good approximation in the frequency range we are considering.

With these definitions, we proceed to evaluate Eq. (37) using Eq. (38) and obtain $\omega^2_{\rm rms} \sim 1.5 \times 10^{-7}(\mu{\rm as/yr})^2$ for nonmemory and $\omega^2_{\rm rms} \sim 10^{-9\pm2}(\mu{\rm as/yr})^2$ for the memory. Again, we note that we consider only the SBBH model in this calculation, and that other GW contributions would further increase these estimates.

We construct an estimator based on survey data, leveraging the above geometric correlation factor. Suppose we have N_p number of celestial objects, $I = 1, 2, \ldots, N_p$, of which we have the data of proper motions: $\omega^i_I(t_p)$ with the corresponding error $\sigma_I(t_p)$, $p = 1, 2, \ldots, N_t$. The data may be recorded as a function of time or could be averaged over an observation period T to a single data point per object (which is the case for Gaia/Theia). We assume that

$$\omega^i_I(t_p) = \omega^i_{I,\rm gw}(t_p) + b^i_I(t_p), \tag{39}$$

where $b^i_I(t_p)$ is the uncorrelated intrinsic motion of the celestial object not related to gravitational waves and $\omega^i_I(t_p)$ is the proper motion data. Here, we clarify the notation. The Latin lowercase indices (i, j) are referring to the directions on sky. The Latin uppercase indices (I, J) are referring to different celestial objects with specific directions $(\boldsymbol{n}, \boldsymbol{n}')$ and we define $\cos\Theta_{IJ} = \boldsymbol{n}\cdot\boldsymbol{n}'$.

We note that each spatial component of $b^i_I(t_p)$ is a Gaussian random variable with standard deviation given by $\sigma_I(t_p)$ with a possible time dependence. Finally, we assume that $b^i_I(t_p) \gg \omega^i_{I,\rm gw}(t_p)$. A consequence of this last assumption is that

$$\langle \omega^i_I(t_p)\omega^j_J(t_q)\rangle \ll \langle \omega^i_I(t_p)\omega_{i,I}(t_p)\rangle = \sigma^2_I(t_p) \tag{40}$$

because $\langle \omega_I^i(t_p)\omega_J^j(t_q)\rangle \sim \langle b_I^i(t_p)b_J^j(t_q)\rangle \sim 0$ and $\langle \omega_I^i(t_p)\omega_{i,I}(t_p)\rangle \sim \langle b_I^i(t_p)b_{i,I}(t_p)\rangle \sim \sigma_I^2(t_p)$. We then construct a likelihood function given by

$$\mathcal{L} \propto \prod_{IJ,p} \exp[-[\omega_{iI}(t_p)\omega_{jJ}(t_p) - \widehat{\omega^2}\Gamma_{ij,\oplus}(\theta_{IJ})] \times [\omega_I^i(t_p)\omega_J^j(t_p) - \widehat{\omega^2}\Gamma_{\oplus}^{ij}(\theta_{IJ})]/(2\sigma_{IJ}^2(t_p))], \quad (41)$$

where $\widehat{\omega^2}$ is what we are trying to estimate [to be compared with Eq. (37)] and $\sigma_{IJ}(t_p)$ is denoting the error in the two-point correlation which we relate to $\omega_I^i(t_p)$ below.

To give an expression for $\sigma_{IJ}(t_p)$, we start with

$$\sigma_{IJ}^2(t_p) = \langle(\omega_I^i(t_p)\omega_J^j(t_p)\omega_{i,I}(t_p)\omega_{j,J}(t_p)\rangle - \langle\omega_I^i(t_p)\omega_J^j(t_p)\rangle\langle\omega_{i,I}(t_p)\omega_{j,J}(t_p)\rangle. \quad (42)$$

Then, utilizing Isserlis's theorem in the first term, we write

$$\langle(\omega_I^i(t_p)\omega_J^j(t_q)\omega_{i,I}(t_p)\omega_{j,J}(t_q)\rangle = 2\langle\omega_I^i(t_p)\omega_J^j(t_q)\rangle\langle\omega_{i,I}(t_p)\omega_{j,J}(t_q)\rangle + \langle\omega_I^i(t_p)\omega_{i,I}(t_p)\rangle\langle\omega_J^j(t_q)\omega_{j,J}(t_q)\rangle. \quad (43)$$

Finally, utilizing Eq. (40), we only retain $\langle\omega_I^i(t_p)\omega_{i,I}(t_p)\rangle\langle\omega_J^j(t_q)\omega_{j,J}(t_q)\rangle$ to write $\sigma_{IJ}^2(t_p) \simeq \sigma_I^4(t_p)$. As a simplification, we take time-independent $\sigma_I(t_p) = \bar{\sigma}$. This relation allows one to relate the confidence interval of Eq. (41) in terms of the number of observed objects and $\bar{\sigma}$. Since the signal-to-noise ratio is expected to scale as $\sqrt{N}/\sigma$, in general, we have

$$\sigma_{\widehat{\omega^2}} \simeq \frac{\bar{\sigma}^2}{\sqrt{N_t N_p(N_p-1)/2}}. \quad (44)$$

Table II summarizes the predicted sensitivities for Gaia and Theia surveys. We assume for both surveys that the dataset consists of a single proper motion measurement for each object over the observation time $T \sim 10$ yr, hence setting $N_t = 1$. In particular, we estimate the sensitivities to $\widehat{\omega^2}$ at the level of 3.0×10^{-2} μas/yr for Gaia and 7.0×10^{-8} μas/yr for Theia.

TABLE II. Proper motion uncertainties in Gaia/Theia datasets for quasistellar objects (QSOs).[a] For Gaia estimates, see Fig. 6 in [141], and for Theia, we use the improvement factors over Gaia in [114,119].

	Gaia	Theia
N_p	10^6	10^8
$\bar{\sigma}$ (μas/yr)	200	3
$\sigma_{\widehat{\omega^2}}$ (μas/yr)^2	3.0×10^{-2}	7.0×10^{-8}

[a]The numbers N_p here are smaller than the total number of objects in these datasets. However, the full dataset has a larger $\bar{\sigma}$ as well. We are considering the subset of the data classified as QSO candidates which have the smallest intrinsic proper motions.

These sensitivities are to be compared with the SBBH estimates of $\omega_{\rm rms}^2 \sim 1.5 \times 10^{-7}$ (μas/yr)^2 for nonmemory and $\omega_{\rm rms}^2 \sim 10^{-9\pm2}$ (μas/yr)^2 for the memory. Therefore, the size of the effect we are considering here is potentially comparable to the nonmemory part and can be potentially detected by Theia.

Two comments are in order. First, the estimate above for Gaia and Theia assumes that all the sources have the same correlated root-mean-square motion. This is certainly not true for a realistic datasets. Second, the usual stochastic nonmemory gravitational wave background contribution has the same angular correlation function as the memory contribution. Therefore, it is not possible to isolate the memory contribution just from the correlation analysis we did above. If the survey samples the peculiar motion many times $N_t \geq 1$ (instead of a single averaged measurement), it would be possible to analyze the two-point correlation in different frequency bins and hence distinguish the memory and nonmemory contributions. In particular, at low frequencies the memory part starts dominating over the nonmemory part due to the different power indices in Eq. (38).

B. Single snapshot analysis

At very low frequencies, the star term ($\Omega_{\rm mem}^{\star} \sim 1/f$) becomes comparable to the Earth memory term ($\Omega_{\rm mem} \sim f$) and cancels it out partially (saturation limit). This relation basically comes from the fact that star term is proportional to the antiderivative of the Earth term which was given by Eq. (20) and the fact that $\Omega(f) \propto h_c^2$. The second scenario outlined before consists of analyzing the very low-frequency limit where the Earth and the star term partially cancel out and we are left with the saturation limit $\delta n_s^i(\infty)$, defined in Eq. (27).

The single snapshot analysis consists of treating the observed angular distribution of the quasars in a CMB-like manner where the quasar density field is characterized by a mean, isotropic density plus a small anisotropic deviation from the mean. The statistics of the two-point correlation of these fluctuations would depend on the galaxy clustering at the time of emission of light as well as propagation effects such as lensing and of course also on the memory accumulation we analyze in this paper. In lieu of a complete analysis hat would take into account all possible sources of quasar clustering, we focus here on a simple estimation of the clustering due to memory and compare it to the expected shot noise due to the finite sample size (number of quasars) available. In this second scenario, since most astrometric deflections will be in the saturation limit, it is straightforward to predict the density pattern (as opposed to

the deflection pattern, since we only have access to a single snapshot). Using Eq. (27) we obtain

$$\rho^{+} \equiv \nabla \cdot \delta \boldsymbol{n}_s^{+}(\infty)(\hat{z}) = -\frac{3}{2} A_0 \cos(2\phi) \sin^2(\theta), \quad (45)$$

$$\rho^{\times} \equiv \nabla \cdot \delta \boldsymbol{n}_s^{\times}(\infty)(\hat{z}) = -\frac{3}{2} A_0 \sin(2\phi) \sin^2(\theta), \quad (46)$$

where the angles are standard spherical coordinates and we assumed a GW signal propagating in the $\hat{z}$ direction. A_0 is the strength of a single GWM signal. In reality, the overdensity will be a sum of many such signals coming from different directions and the full effect will be on the order of the memory as estimated in the right part of Fig. 5, i.e., $A_0 \simeq h_c$.

Assuming an isotropic initial distribution, we plot the correlation functions for this limit defined in Eq. (34) in the bottom row of Fig. 7. We also plot a random realization of these density perturbations in the saturation limit in Fig. 8. The fact that there is a $\rho \propto \sin^2(\theta)$ dependence on the right-hand side implies that the astrometric deflections in the saturation limit are contributing only at the $l = 2$ multipole level in the spherical harmonic expansion of the density fluctuation field. More specifically, expanding the smoothed quasar overdensity in spherical harmonics, we get

$$\rho^A = a^A_{lm} Y_{lm}(\theta, \phi), \quad (47)$$

where $\langle a^A_{lm} \rangle = 0$ and $C_l = \langle |a^+_{lm}|^2 + |a^\times_{lm}|^2 \rangle$. The strain memory we estimated in Sec. IV is around $10^{-(10\text{–}11)}$ for the dominant SBBH contribution. That implies a value for the C_2 coefficient of about $C_2 \sim 10^{-(20\text{–}22)}$. The measurement of this coefficient is limited by the Poisson shot noise due to the limited sample size. For finite angular distributions, the shot noise is l independent and given by [142] $C_{l,\text{shot}} = \frac{4\pi}{N}(1 - \delta_{l0})$, which implies that one would need at least 10^{20} number of light sources to sufficiently suppress it. Since even the most ambitious astrometric observations such as Theia have a projected sample size of about 10^9 astronomical objects, we conclude that it is unlikely that such an anisotropy could be detected. Additionally, since the memory affects the low multipole moment, the measurement of C_2 is cosmic variance limited and, hence, any other more significant effect that modifies the C_2 coefficient cannot be subtracted from the theoretical expectation to a greater than $\mathcal{O}(1)$ precision. This makes the measurement of a subdominant effect, such as due to the memory, unlikely. For this reason, our calculation can be understood as a proof of principle about the potential of the memory to affect the anisotropy of the Universe, but realistically, an observable signature would require a much more powerful source of memory than the ones we study in the present work.

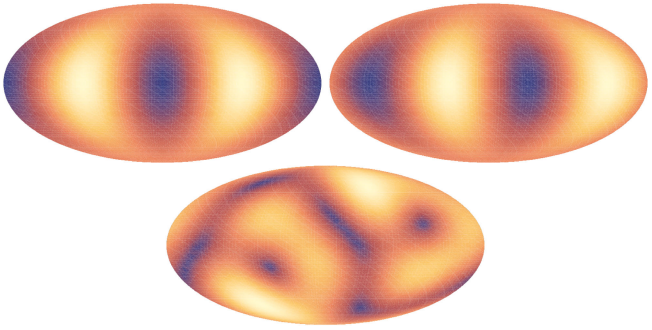

FIG. 8. Top row: density patterns of + and × polarization of $\delta \boldsymbol{n}_s^{+,\times}$, respectively, for a GW propagating in the $\hat{z}$ direction. Bottom: a realization of the density pattern for many such GWs uniformly distributed in direction and polarization.

Before closing this section, we would like to stress the limits of our calculation. Our implicit assumption of GW planar wavefronts implies that the GW sources are at a much greater redshift than the sources of light we consider. However, in the list of the presently observed quasars, most are at a distance of $z \sim \mathcal{O}(1)$ [119]. As a result, considering sources of GWs even further away would dramatically decrease the overall memory buildup. Instead, the better option would be to limit a potential analysis to the subgroup of quasars that are closer than $z \leq 1$, therefore allowing for a longer memory buildup while our approximation of planar wavefronts holds. This overall would imply a decrease of the total quasars available to 25% which would decrease the result estimated above by an order of magnitude. Understanding the optimal trade-off between the number of quasars and duration of memory buildup or performing an improved calculation with spherical wavefronts as in [139] is left for future work.

VI. DISCUSSION AND CONCLUSIONS

The memory effect is one of the most intriguing, as of now unconfirmed, predictions of general relativity. Unfortunately, direct detection efforts of the memory effect have been hampered so far due to the low-frequency insensitivity of current ground-based detectors. Alternative approaches that have been suggested for exploring the effects of memory focus on space-based detectors or astrometry. In either case, one is faced with the challenge of isolating the memory signal in the face of a typically dominant primary GW signal. In this work, we explore whether one can leverage one of the fundamental differences between the primary and the memory signals to distinguish their phenomenology: namely, the primary signal is transient, whereas the memory signal is permanent. One would expect that, over a long period of time, the small but permanent memory signals coming from different sources from different directions in the sky would add up in a random walk fashion and produce an effect that is ever increasing and potentially greater than even the present primary signals. We refer to this concept as "accumulating

memory" and the purpose of this work was to explore the consequences of such an effect in the case of astrometry.

Even though, in principle, every possible GW source should contribute to the effect described above, we focused in this work on GWs coming from compact binary coalescences because these mergers produce some of the strongest GWs possible and also because their merger rates and mass distributions can be modeled even at high redshift, which is necessary for computing the GWM accumulation. Using this information, we provided the formalism for computing the accumulated GWM strain and derived the total GWM accumulation over the history of the Universe from compact binary coalescences.

Subsequently, we expanded upon the work of Madison [49] on astrometric deflections from GWM by estimating the effect arising from many GW sources over the entire Universe and separated the detection prospects into different scenarios: observations of the proper motions of distant objects and a single snapshot observation of the angular distribution of very far away sources such as quasars. For the first case, we found that the Earth term dominates and indicated that the angular correlation function of the proper motion of light sources should be the conventional one originally derived by Book and Flanagan [139]. Within this scenario, we constructed memory SGWB sampled from realistic models of various binary populations and estimated the amplitude of apparent proper motions that would be induced by gravitational wave memory. In the latter scenario, we found that both the Earth and star terms (analogous to the integrated Sachs-Wolfe effect for the CMB) contribute at the same level and the overall deflection would be dominated by GWs in the saturation limit, which consists of the Earth and star terms obtaining their maximum value. We derived the new angular correlation function for this limit and assessed the detection prospects with experiments such as Gaia and Theia. Our findings indicate that, while it may be possible to detect the memory contribution to the proper motion of distant light sources, it is highly unlikely that the second scenario could be observationally confirmed.

ACKNOWLEDGMENTS

The authors would like to thank Colm Talbot for valuable conversations at an early part of this work. A. P. would like to thank Javier Carrón Duque for insightful comments. A. P. was supported by IBS under the project code, IBS-R018-D1. A. P. acknowledges support from the "Consolidación Investigadora" Grant No. CNS2022-135590. The work of A. P. is partially supported by the Spanish Research Agency (Agencia Estatal de Investigación) through the Grant IFT Centro de Excelencia Severo Ochoa No. CEX2020-001007-S, funded by MCIN/AEI/10.13039/501100011033. T. B. was in part supported by the McKnight award at the University of Minnesota. V. M. was in part supported by the NSF Grant No. PHY-2110238.

[1] J. Aasi *et al.*, Advanced LIGO, Classical Quantum Gravity **32**, 074001 (2015).
[2] F Acernese *et al.*, Advanced Virgo: A second-generation interferometric gravitational wave detector, Classical Quantum Gravity **32**, 024001 (2015).
[3] B. P. Abbott *et al.*, Observation of gravitational waves from a binary black hole merger, Phys. Rev. Lett. **116**, 061102 (2016).
[4] B. P. Abbott *et al.*, Gw170817: Observation of gravitational waves from a binary neutron star inspiral, Phys. Rev. Lett. **119**, 161101 (2017).
[5] R. Abbott *et al.*, Observation of gravitational waves from two neutron star–black hole coalescences, Astrophys. J. Lett. **915**, L5 (2021).
[6] G. Agazie *et al.* (NANOGrav Collaboration), The NANOGrav 15 yr data set: Evidence for a gravitational-wave background, Astrophys. J. Lett. **951**, L8 (2023).
[7] J. Antoniadis *et al.* (EPTA Collaboration), The second data release from the European pulsar timing array III. Search for gravitational wave signals, Astron. Astrophys. **678**, A50 (2023).
[8] D. J. Reardon *et al.*, Search for an isotropic gravitational-wave background with the Parkes pulsar timing array, Astrophys. J. Lett. **951**, L6 (2023).
[9] H. Xu *et al.*, Searching for the nano-hertz stochastic gravitational wave background with the Chinese pulsar timing array data release I, Res. Astron. Astrophys. **23**, 075024 (2023).
[10] B. P. Abbott *et al.*, Tests of general relativity with GW150914, Phys. Rev. Lett. **116**, 221101 (2016).
[11] R. Abbott *et al.*, Tests of general relativity with GWTC-3, arXiv:2112.06861 [Phys. Rev. D (to be published)].
[12] B. P. Abbott *et al.*, A gravitational-wave standard siren measurement of the Hubble constant, Nature (London) **551**, 85 (2017).
[13] R. Abbott *et al.*, Constraints on the cosmic expansion history from GWTC-3, Astrophys. J. **949**, 76 (2023).
[14] B. P. Abbott *et al.*, GW150914: Implications for the stochastic gravitational-wave background from binary black holes, Phys. Rev. Lett. **116**, 131102 (2016).
[15] R. Abbott *et al.*, The population of merging compact binaries inferred using gravitational waves through GWTC-3, Phys. Rev. X **13**, 011048 (2023).
[16] B. P. Abbott *et al.*, GW170817: Implications for the stochastic gravitational-wave background from compact binary coalescences, Phys. Rev. Lett. **120**, 091101 (2018).
[17] V. Mandic, S. Bird, and I. Cholis, Stochastic gravitational-wave background due to primordial binary black hole mergers, Phys. Rev. Lett. **117**, 201102 (2016).

[18] J. Antoniadis *et al.* (EPTA Collaboration), The second data release from the European pulsar timing array: V. Implications for massive black holes, dark matter and the early Universe, Astron. Astrophys. **685**, A94 (2024).
[19] R. Abbott *et al.*, GWTC-3: Compact binary coalescences observed by LIGO and Virgo during the second part of the third observing run, Phys. Rev. X **13**, 041039 (2023).
[20] B. Goncharov, L. Donnay, and J. Harms, Inferring fundamental spacetime symmetries with gravitational-wave memory: From LISA to the Einstein telescope, Phys. Rev. Lett. **132**, 241401 (2024).
[21] A. M. Grant and D. A. Nichols, Outlook for detecting the gravitational-wave displacement and spin memory effects with current and future gravitational-wave detectors, Phys. Rev. D **107**, 064056 (2023).
[22] M. Hübner, C. Talbot, P. D. Lasky, and E. Thrane, Measuring gravitational-wave memory in the first LIGO/Virgo gravitational-wave transient catalog, Phys. Rev. D **101**, 023011 (2020).
[23] A. M. Grant and D. A. Nichols, Outlook for detecting the gravitational-wave displacement and spin memory effects with current and future gravitational-wave detectors, Phys. Rev. D **107**, 064056 (2023); **108**, 029901(E) (2023).
[24] M. Favata, The gravitational-wave memory effect, Classical Quantum Gravity **27**, 084036 (2010).
[25] S. Ghosh, A. Weaver, J. Sanjuan, P. Fulda, and G. Mueller, Detection of the gravitational memory effect in LISA using triggers from ground-based detectors, Phys. Rev. D **107**, 084051 (2023).
[26] S. Gasparotto, R. Vicente, D. Blas, A. C. Jenkins, and E. Barausse, Can gravitational-wave memory help constrain binary black-hole parameters? A LISA case study, Phys. Rev. D **107**, 124033 (2023).
[27] G. Agazie *et al.*, The NANOGrav 12.5-year data set: Search for gravitational wave memory, Astrophys. J. **963**, 61 (2024).
[28] V. B. Braginsky and L. P. Grishchuk, Kinematic resonance and memory effect in free mass gravitational antennas, Sov. Phys. JETP **62**, 427 (1985).
[29] Y. B. Zel'dovich and A. G. Polnarev, Radiation of gravitational waves by a cluster of superdense stars, Sov. Astron. **18**, 17 (1974).
[30] V. B. Braginsky and K. S. Thorne, Gravitational-wave bursts with memory and experimental prospects, Nature (London) **327**, 123 (1987).
[31] L. Blanchet and T. Damour, Hereditary effects in gravitational radiation, Phys. Rev. D **46**, 4304 (1992).
[32] K. S. Thorne, Gravitational-wave bursts with memory: The Christodoulou effect, Phys. Rev. D **45**, 520 (1992).
[33] L. Bieri and D. Garfinkle, An electromagnetic analogue of gravitational wave memory, Classical Quantum Gravity **30**, 195009 (2013).
[34] L. Bieri and D. Garfinkle, Perturbative and gauge invariant treatment of gravitational wave memory, Phys. Rev. D **89**, 084039 (2014).
[35] A. Tolish and R. M. Wald, Retarded fields of null particles and the memory effect, Phys. Rev. D **89**, 064008 (2014).
[36] A. Tolish, L. Bieri, D. Garfinkle, and R. M. Wald, Examination of a simple example of gravitational wave memory, Phys. Rev. D **90**, 044060 (2014).
[37] A. Tolish and R. M. Wald, Cosmological memory effect, Phys. Rev. D **94**, 044009 (2016).
[38] D. Garfinkle, S. Hollands, A. Ishibashi, A. Tolish, and R. M. Wald, The memory effect for particle scattering in even spacetime dimensions, Classical Quantum Gravity **34**, 145015 (2017).
[39] L. Bieri, D. Garfinkle, and N. Yunes, Gravitational wave memory in ΛCDM cosmology, Classical Quantum Gravity **34**, 215002 (2017).
[40] L. Bieri, New effects in gravitational waves and memory, Phys. Rev. D **103**, 024043 (2021).
[41] N. Jokela, K. Kajantie, and M. Sarkkinen, Gravitational wave memory and its tail in cosmology, Phys. Rev. D **106**, 064022 (2022).
[42] A. Strominger and A. Zhiboedov, Gravitational memory, BMS supertranslations and soft theorems, J. High Energy Phys. 01 (2016) 086.
[43] C. Talbot, E. Thrane, P. D. Lasky, and F. Lin, Gravitational-wave memory: Waveforms and phenomenology, Phys. Rev. D **98**, 064031 (2018).
[44] A. C. Jenkins and M. Sakellariadou, Nonlinear gravitational-wave memory from cusps and kinks on cosmic strings, Classical Quantum Gravity **38**, 165004 (2021).
[45] L. O. McNeill, E. Thrane, and P. D. Lasky, Detecting gravitational wave memory without parent signals, Phys. Rev. Lett. **118**, 181103 (2017).
[46] B. Allen, Gravitational wave stochastic background from cosmological particle decay, Phys. Rev. Res. **2**, 012034 (2020).
[47] Z.-C. Zhao and Z. Cao, Stochastic gravitational wave background due to gravitational wave memory, Sci. China Phys. Mech. Astron. **65**, 119511 (2022).
[48] Z. Cao, X. He, and Z.-C. Zhao, Gravitational wave memory produced by cosmic background radiation, Phys. Lett. B **847**, 138313 (2023).
[49] D. R. Madison, Persistent astrometric deflections from gravitational-wave memory, Phys. Rev. Lett. **125**, 041101 (2020).
[50] D. R. Madison, Framework for describing perturbations to the cosmic microwave background from a gravitational wave burst with memory, Phys. Rev. D **103**, 083515 (2021).
[51] L. P. Grishchuk, Amplification of gravitational waves in an isotropic universe, Sov. J. Exp. Theor. Phys. **40**, 409 (1975).
[52] R. Bar-Kana, Limits on direct detection of gravitational waves, Phys. Rev. D **50**, 1157 (1994).
[53] A. A. Starobinskiĭ, Spectrum of relict gravitational radiation and the early state of the Universe, JETP Lett. **30**, 682 (1979).
[54] M. Turner, Detectability of inflation-produced gravitational waves, Phys. Rev. D **55**, R435 (1997).
[55] N. Barnaby, E. Pajer, and M. Peloso, Gauge field production in axion inflation: Consequences for monodromy, non-Gaussianity in the CMB, and gravitational waves at interferometers, Phys. Rev. D **85**, 023525 (2012).
[56] N. Seto and A. Taruya, Measuring a parity-violation signature in the early Universe via ground-based laser interferometers, Phys. Rev. Lett. **99**, 121101 (2007).

[57] M. C. Guzzetti, N. Bartolo, M. Liguori, and S. Matarrese, Gravitational waves from inflation, Riv. Nuovo Cimento **39**, 399 (2016).
[58] E. Witten, Cosmic separation of phases, Phys. Rev. D **30**, 272 (1984).
[59] C. J. Hogan, Gravitational radiation from cosmological phase transitions, Mon. Not. R. Astron. Soc. **218**, 629 (1986).
[60] M. S. Turner and F. Wilczek, Relic gravitational waves and extended inflation, Phys. Rev. Lett. **65**, 3080 (1990).
[61] A. Kosowsky, M. S. Turner, and R. Watkins, Gravitational waves from first-order cosmological phase transitions, Phys. Rev. Lett. **69**, 2026 (1992).
[62] M. Kamionkowski, A. Kosowsky, and M. S. Turner, Gravitational radiation from first-order phase transitions, Phys. Rev. D **49**, 2837 (1994).
[63] R. Apreda, M. Maggiore, A. Nicolis, and A. Riotto, Gravitational waves from electroweak phase transitions, Nucl. Phys. **B631**, 342 (2002).
[64] C. Caprini, R. Durrer, and G. Servant, Gravitational wave generation from bubble collisions in first-order phase transitions: An analytic approach, Phys. Rev. D **77**, 124015 (2008).
[65] P. Binétruy, A. Bohé, C. Caprini, and J.-F. Dufaux, Cosmological backgrounds of gravitational waves and eLISA/NGO: Phase transitions, cosmic strings and other sources, J. Cosmol. Astropart. Phys. 06 (2012) 027.
[66] C. Caprini *et al.*, Science with the space-based interferometer eLISA. II: Gravitational waves from cosmological phase transitions, J. Cosmol. Astropart. Phys. 04 (2016) 001.
[67] L. Boyle and A. Buonanno, Relating gravitational wave constraints from primordial nucleosynthesis, pulsar timing, laser interferometers, and the CMB: Implications for the early Universe, Phys. Rev. D **78**, 043531 (2008).
[68] R. Caldwell and B. Allen, Cosmological constraints on cosmic-string gravitational radiation, Phys. Rev. D **45**, 3447 (1992).
[69] T. Damour and A. Vilenkin, Gravitational wave bursts from cosmic strings, Phys. Rev. Lett. **85**, 3761 (2000).
[70] T. Damour and A. Vilenkin, Gravitational radiation from cosmic (super)strings: Bursts, stochastic background, and observational windows, Phys. Rev. D **71**, 063510 (2005).
[71] X. Siemens, V. Mandic, and J. Creighton, Gravitational-wave stochastic background from cosmic strings, Phys. Rev. Lett. **98**, 111101 (2007).
[72] S. Ölmez, V. Mandic, and X. Siemens, Gravitational-wave stochastic background from kinks and cusps on cosmic strings, Phys. Rev. D **81**, 104028 (2010).
[73] X. Siemens, J. Creighton, I. Maor, S. R. Majumder, K. Cannon, and J. Read, Gravitational wave bursts from cosmic (super)strings: Quantitative analysis and constraints, Phys. Rev. D **73**, 105001 (2006).
[74] L. Lorenz, C. Ringeval, and M. Sakellariadou, Cosmic string loop distribution on all length scales and at any redshift, J. Cosmol. Astropart. Phys. 10 (2010) 003.
[75] J. J. Blanco-Pillado, K. D. Olum, and B. Shlaer, Number of cosmic string loops, Phys. Rev. D **89**, 023512 (2014).
[76] B. P. Abbott *et al.*, Constraints on cosmic strings using data from the first Advanced LIGO observing run, Phys. Rev. D **97**, 102002 (2018).
[77] R. Abbott *et al.*, Constraints on cosmic strings using data from the third Advanced LIGO–Virgo observing run, Phys. Rev. Lett. **126**, 241102 (2021).
[78] D. J. Weir, Gravitational waves from a first order electroweak phase transition: A brief review, Phil. Trans. R. Soc. A **376**, 20170126 (2018).
[79] E. Phinney, The rate of neutron star binary mergers in the Universe: Minimal predictions for gravity wave detectors, Astrop. J. **380**, L17 (1991), https://articles.adsabs.harvard.edu/full/1991ApJ...380L..17P.
[80] T. Regimbau and J. A. de Freitas Pacheco, Stochastic background from coalescences of neutron star–neutron star binaries, Astrophys. J. **642**, 455 (2006).
[81] X.-J. Zhu, E. Howell, T. Regimbau, D. Blair, and Z.-H. Zhu, Stochastic gravitational wave background from coalescing binary black holes, Astrophys. J. **739**, 86 (2011).
[82] S. Marassi, R. Schneider, G. Corvino, V. Ferrari, and S. P. Zwart, Imprint of the merger and ring-down on the gravitational wave background from black hole binaries coalescence, Phys. Rev. D **84**, 124037 (2011).
[83] P. A. Rosado, Gravitational wave background from binary systems, Phys. Rev. D **84**, 084004 (2011).
[84] T. Regimbau and V. Mandic, Astrophysical sources of a stochastic gravitational-wave background, Classical Quantum Gravity **25**, 184018 (2008).
[85] C. Wu, V. Mandic, and T. Regimbau, Accessibility of the gravitational-wave background due to binary coalescences to second and third generation gravitational-wave detectors, Phys. Rev. D **85**, 104024 (2012).
[86] C. Cutler, Gravitational waves from neutron stars with large toroidal *b* fields, Phys. Rev. D **66**, 084025 (2002).
[87] S. Bonazzola and E. Gourgoulhon, Gravitational waves from pulsars: Emission by the magnetic field induced distortion, Astron. Astrop. **312**, 675 (1996), https://adsabs.harvard.edu/full/1996A%26A...312..675B.
[88] S. Marassi, R. Ciolfi, R. Schneider, L. Stella, and V. Ferrari, Stochastic background of gravitational waves emitted by magnetars, Mon. Not. R. Astron. Soc. **411**, 2549 (2011).
[89] B. J. Owen, L. Lindblom, C. Cutler, B. F. Schutz, A. Vecchio, and N. Andersson, Gravitational waves from hot Young rapidly rotating neutron stars, Phys. Rev. D **58**, 084020 (1998).
[90] T. Regimbau and J. de Freitas Pacheco, Cosmic background of gravitational waves from rotating neutron stars, Astron. Astrophys. **376**, 381 (2001).
[91] J. L. Houser, J. M. Centrella, and S. C. Smith, Gravitational radiation from nonaxisymmetric instability in a rotating star, Phys. Rev. Lett. **72**, 1314 (1994).
[92] D. Lai and S. Shapiro, Gravitational radiation from rapidly rotating nascent neutron stars, Astrop. J. **442**, 259 (1995), https://articles.adsabs.harvard.edu/full/1995ApJ...442..259L.
[93] C.-J. Wu, V. Mandic, and T. Regimbau, Accessibility of the stochastic gravitational wave background from magnetars to the interferometric gravitational wave detectors, Phys. Rev. D **87**, 042002 (2013).
[94] T. Regimbau, The astrophysical gravitational wave stochastic background, Res. Astron. Astrophys. **11**, 369 (2011).

[95] D. M. Coward, R. R. Burman, and D. G. Blair, Simulating a stochastic background of gravitational waves from neutron star formation at cosmological distances, Mon. Not. R. Astron. Soc. **329**, 411 (2002).
[96] S. Marassi, R. Schneider, and V. Ferrari, Gravitational wave backgrounds and the cosmic transition from population III to population II stars, Mon. Not. R. Astron. Soc. **398**, 293 (2009).
[97] P. Sandick, K. A. Olive, F. Daigne, and E. Vangioni, Gravitational waves from the first stars, Phys. Rev. D **73**, 104024 (2006).
[98] A. Buonanno, G. Sigl, G. G. Raffelt, H.-T. Janka, and E. Müller, Stochastic gravitational-wave background from cosmological supernovae, Phys. Rev. D **72**, 084001 (2005).
[99] K. Crocker, V. Mandic, T. Regimbau, K. Belczynski, W. Gladysz, K. Olive, T. Prestegard, and E. Vangioni, Model of the stochastic gravitational-wave background due to core collapse to black holes, Phys. Rev. D **92**, 063005 (2015).
[100] K. Crocker, T. Prestegard, V. Mandic, T. Regimbau, K. Olive, and E. Vangioni, Systematic study of the stochastic gravitational-wave background due to stellar core collapse, Phys. Rev. D **95**, 063015 (2017).
[101] B. Finkel, H. Andresen, and V. Mandic, Stochastic gravitational-wave background from stellar core-collapse events, Phys. Rev. D **105**, 063022 (2022).
[102] R. Abbott *et al.* (LIGO Scientific, Virgo, and KAGRA Collaborations), Constraints on cosmic strings using data from the third Advanced LIGO–Virgo observing run, Phys. Rev. Lett. **126**, 241102 (2021).
[103] R. Abbott *et al.* (KAGRA, VIRGO, and LIGO Scientific Collaborations), Population of merging compact binaries inferred using gravitational waves through GWTC-3, Phys. Rev. X **13**, 011048 (2023).
[104] R. Abbott *et al.* (LIGO Scientific, VIRGO, and KAGRA Collaborations), GWTC-3: Compact binary coalescences observed by LIGO and Virgo during the second part of the third observing run, Phys. Rev. X **13**, 041039 (2023).
[105] M. Enoki, K. T. Inoue, M. Nagashima, and N. Sugiyama, Gravitational waves from supermassive black hole coalescence in a hierarchical galaxy formation model, Astrophys. J. **615**, 19 (2004).
[106] M. Raidal, V. Vaskonen, and H. Veermäe, Gravitational waves from primordial black hole mergers, J. Cosmol. Astropart. Phys. 09 (2017) 037.
[107] G. Collaboration *et al.*, The Gaia mission, Astron. Astrophys. **595**, A1 (2016).
[108] A. G. Brown, A. Vallenari, T. Prusti, J. De Bruijne, C. Babusiaux, M. Biermann, O. Creevey, D. Evans, L. Eyer, A. Hutton *et al.*, Gaia early data release 3-summary of the contents and survey properties, Astron. Astrophys. **649**, A1 (2021).
[109] L. Lindegren, S. Klioner, J. Hernández, A. Bombrun, M. Ramos-Lerate, H. Steidelmüller, U. Bastian, M. Biermann, A. de Torres, E. Gerlach *et al.*, Gaia early data release 3-the astrometric solution, Astron. Astrophys. **649**, A2 (2021).
[110] A. Vallenari, A. Brown, T. Prusti, J. de Bruijne, F. Arenou, C. Babusiaux, M. Biermann, O. Creevey, C. Ducourant, D. Evans *et al.*, Gaia data release 3-summary of the content and survey properties, Astron. Astrophys. **674**, A1 (2023).
[111] C. Babusiaux, C. Fabricius, S. Khanna, T. Muraveva, C. Reylé, F. Spoto, A. Vallenari, X. Luri, F. Arenou, M. Álvarez *et al.*, Gaia data release 3-catalogue validation, Astron. Astrophys. **674**, A32 (2023).
[112] C. Boehm, A. Krone-Martins, A. Amorim, G. Anglada-Escude, A. Brandeker, F. Courbin, T. Ensslin, A. Falcao, K. Freese, B. Holl *et al.*, Theia: Faint objects in motion or the new astrometry frontier, arXiv:1707.01348.
[113] F. Malbet *et al.*, Theia: Science cases and mission profiles for high precision astrometry in the future, in SPIE Astronomical Telescopes + Instrumentation 2022 (2022), arXiv:2207.12540.
[114] J. Garcia-Bellido, H. Murayama, and G. White, Exploring the early Universe with Gaia and Theia, J. Cosmol. Astropart. Phys. 12 (2021) 023.
[115] C. J. Moore, D. P. Mihaylov, A. Lasenby, and G. Gilmore, Astrometric search method for individually resolvable gravitational wave sources with Gaia, Phys. Rev. Lett. **119**, 261102 (2017).
[116] S. A. Klioner, Gaia-like astrometry and gravitational waves, Classical Quantum Gravity **35**, 045005 (2018).
[117] D. P. Mihaylov, C. J. Moore, J. R. Gair, A. Lasenby, and G. Gilmore, Astrometric effects of gravitational wave backgrounds with non-Einsteinian polarizations, Phys. Rev. D **97**, 124058 (2018).
[118] D. P. Mihaylov, C. J. Moore, J. Gair, A. Lasenby, and G. Gilmore, Astrometric effects of gravitational wave backgrounds with nonluminal propagation speeds, Phys. Rev. D **101**, 024038 (2020).
[119] S. Jaraba, J. García-Bellido, S. Kuroyanagi, S. Ferraiuolo, and M. Braglia, Stochastic gravitational wave background constraints from Gaia DR3 astrometry, Mon. Not. R. Astron. Soc. **524**, 3609 (2023).
[120] B. P. Abbott, R. Abbott, T. Abbott, M. Abernathy, F. Acernese, K. Ackley, C. Adams, T. Adams, P. Addesso, R. Adhikari *et al.*, GW150914: Implications for the stochastic gravitational-wave background from binary black holes, Phys. Rev. Lett. **116**, 131102 (2016).
[121] E. Phinney, A practical theorem on gravitational wave backgrounds, arXiv:astro-ph/0108028.
[122] L. Hernquist and V. Springel, An analytical model for the history of cosmic star formation, Mon. Not. R. Astron. Soc. **341**, 1253 (2003).
[123] R. Abbott, T. Abbott, F. Acernese, K. Ackley, C. Adams, N. Adhikari, R. Adhikari, V. Adya, C. Affeldt, D. Agarwal *et al.*, Population of merging compact binaries inferred using gravitational waves through GWTC-3, Phys. Rev. X **13**, 011048 (2023).
[124] K. Inomata, M. Kawasaki, K. Mukaida, Y. Tada, and T. T. Yanagida, Inflationary primordial black holes as all dark matter, Phys. Rev. D **96**, 043504 (2017).
[125] M. Raidal, C. Spethmann, V. Vaskonen, and H. Veermäe, Formation and evolution of primordial black hole binaries in the early Universe, J. Cosmol. Astropart. Phys. 02 (2019) 018.
[126] J. Flitter, J. B. Muñoz, and E. D. Kovetz, Outliers in the LIGO black hole mass function from coagulation in dense clusters, Mon. Not. R. Astron. Soc. **507**, 743 (2021).

[127] A. Dolgov and J. Silk, Baryon isocurvature fluctuations at small scales and baryonic dark matter, Phys. Rev. D **47**, 4244 (1993).
[128] Y. Ali-Haïmoud, E. D. Kovetz, and M. Kamionkowski, Merger rate of primordial black-hole binaries, Phys. Rev. D **96**, 123523 (2017).
[129] V. Vaskonen and H. Veermäe, Lower bound on the primordial black hole merger rate, Phys. Rev. D **101**, 043015 (2020).
[130] V. Atal, A. Sanglas, and N. Triantafyllou, LIGO/Virgo black holes and dark matter: The effect of spatial clustering, J. Cosmol. Astropart. Phys. 11 (2020) 036.
[131] S. Mukherjee and J. Silk, Can we distinguish astrophysical from primordial black holes via the stochastic gravitational wave background?, Mon. Not. R. Astron. Soc. **506**, 3977 (2021).
[132] V. Mandic, S. Bird, and I. Cholis, Stochastic gravitational-wave background due to primordial binary black hole mergers, Phys. Rev. Lett. **117**, 201102 (2016).
[133] S. Clesse and J. Garcia-Bellido, GW190425, GW190521 and GW190814: Three candidate mergers of primordial black holes from the QCD epoch, Phys. Dark Universe **38**, 101111 (2022).
[134] G. Franciolini, V. Baibhav, V. De Luca, K. K. Ng, K. W. Wong, E. Berti, P. Pani, A. Riotto, and S. Vitale, Searching for a subpopulation of primordial black holes in LIGO-Virgo gravitational-wave data, Phys. Rev. D **105**, 083526 (2022).
[135] S. Chen, A. Sesana, and C. J. Conselice, Constraining astrophysical observables of galaxy and supermassive black hole binary mergers using pulsar timing arrays, Mon. Not. R. Astron. Soc. **488**, 401 (2019).
[136] H. Middleton, W. Del Pozzo, W. M. Farr, A. Sesana, and A. Vecchio, Astrophysical constraints on massive black hole binary evolution from pulsar timing arrays, Mon. Not. R. Astron. Soc. **455**, L72 (2015).
[137] N. Steinle, H. Middleton, C. J. Moore, S. Chen, A. Klein, G. Pratten, R. Buscicchio, E. Finch, and A. Vecchio, Implications of pulsar timing array observations for LISA detections of massive black hole binaries, Mon. Not. R. Astron. Soc. **525**, 2851 (2023).
[138] H. Middleton, S. Chen, W. Del Pozzo, A. Sesana, and A. Vecchio, No tension between assembly models of super massive black hole binaries and pulsar observations, Nat. Commun. **9**, 573 (2018).
[139] L. G. Book and E. E. Flanagan, Astrometric effects of a stochastic gravitational wave background, Phys. Rev. D **83**, 024024 (2011).
[140] G. Agazie, A. Anumarlapudi, A. M. Archibald, P. T. Baker, B. Bécsy, L. Blecha, A. Bonilla, A. Brazier, P. R. Brook, S. Burke-Spolaor *et al.*, The nanograv 15 yr data set: Constraints on supermassive black hole binaries from the gravitational-wave background, Astrophys. J. Lett. **952**, L37 (2023).
[141] J. Paine, J. Darling, and A. Truebenbach, The Gaia–WISE extragalactic astrometric catalog, Astrophys. J. Suppl. Ser. **236**, 37 (2018).
[142] S. S. Campbell, Angular power spectra with finite counts, Mon. Not. R. Astron. Soc. **448**, 2854 (2015).